Flood Risk and Climate Change Hokkaido

WP1 Climate change

Client

Partners for Water

Flood Risk and Climate Change Hokkaido

WP1 Climate change

Draft report

Authors
Hoshino, Tsuyoshi (Hokkaido Unversity)
Hegnauer, Mark (Deltares)
Shimizu, Keita (Hokkaido Unversity)
Yamada, Tomohito (Hokkaido Unversity)

PR3983.10
December 2021

Table of contents

1 Introduction

The increasing risk of heavy rainfall due to climate change is of great importance and is a challenge for countries of the world. In recent years, the assessment of heavy rainfall risk considering climate change has been realized by using future projections based on climate models (e.g., Yamada et al., 2018, Yamada, 2019). Various models have been used to assess the risk of heavy rainfall, such as the climate projection model, rainfall-runoff model, levee breaching model, flooding model, and damage assessment model for loss of life and economic damage. However, there are various uncertainties inherent in these models because the number of disaster cases that we have experienced is limited. The development of these models and the methodology of risk assessment are being studied in many countries. In order to develop objective and reliable risk assessment methods, it is necessary for countries around the world that are making advanced efforts in heavy rainfall risk assessment and flood control measures to compare their risk assessment methodology with each other and develop them jointly. For this reason, a joint research project called "Flood risk and climate change Hokkaido" has been started by research groups in Japan and the Netherlands.

The joint research project is based on the ensemble approach for climate change projection and risk assessment led by Japan (e.g., Yamada et al., 2018, Hoshino et al., 2020). In this approach, a 5km-resolution large ensemble climate dataset was used to estimate the physical characteristics of extreme rainfall under past and future climate conditions. Results from flood risk assessment based on the ensemble climate data clarified that extreme heavy rainfall in future climate could occur more frequently compare to the past climate and extreme rainfall will be stronger in the future climate and more intense both in temporal and spatial scales, and flood risk will be higher in the future (Yamada, 2019). The flood risk assessment considered the variability of the climate system which caused extreme heavy rainfall in both past and future climate using thousands years of climate simulations. In addition, the ensemble information derived from huge model calculations is also supported by statistical theory (Shimizu et al., 2020). Our history represents only one outcome of a range of climate variability. One of the important concepts from the risk-based methodology based on ensemble information is that it proceeds under "two wheels" constructed from physics and statistical theory (Figure-1). In recent years, these achievements are now used to discuss future flood control policy considering climate change at a national level in Japan, although flood control management was traditionally based on historical information in Japan.

On the other hand, the Netherlands has pioneered the social implementation of risk-based flood control measure. Specifically, the Netherlands adopted a risk-based approach that integrated flood damage and its occurrence probability (J. Van, 2016). Their flood control measure has assumed evacuation rates for residents by each region (B. Kolen, 2013) and quantified the human and economic damage associated with levee breaches (S.N. Jonkman, 2007, B. Maaskant, 2009). Based on this risk-based approach, a policy decision has been made to reduce the risk of mortality from flood inundation to less than 10^{-5} by 2050 for the entire Netherlands (KNMI and Deltares, 2015; The Ministry of infrastructure and Environment and The Ministry of Economic Affairs, 2015). Under the support of "Partner for waters", a collaborate research with Academia, Industry and Government promoted by Netherlands Enterprise Agency, has been started to integrate knowledge from the two countries.

In the field of flood control, hydrological models (rainfall-runoff, river flow and inundation model) that describe the processes from rainfall to inundation play a fundamental role in planning the design river discharge and flood damage. However, the model parameters are subject to uncertainty due to the limited number of observed flood events. In "working package 1 (WP1)" of this joint research,

the relationship between rainfall and peak discharge expressed by each model is considered as an important factor to clarify uncertainty inherent in a model itself. The advantage of quantifying rainfall-peak discharge relation is the estimation of uncertainty included in different hydrological models and parameter settings. In addition, future changes in the spatio-temporal characteristics of extreme rainfalls with low frequency can be incorporated in the peak discharge estimation by introducing the rainfall-peak discharge relation expressed by models. The purpose of WP1 is to construct a rational framework to make probability information of peak discharge incorporating uncertainty of rainfall-runoff model and spatio-temporal rainfall pattern. The output of WP1 is a probability distribution of peak discharge of each return period. Derivation of probable information of peak discharge requires two types of information. One is a frequency distribution of rainfall volume of each return period, and another is the rainfall-peak discharge relation derived from rainfall-runoff models. The advantage of this methodology is that the estimated peak discharge can be updated in accordance with the differences and sophistication of climate models and rainfall-runoff models. This technical report describes the methodology and results developed in WP1.

Figure 1 The concept of risk-based approach constructed from "two wheels" (Yamada et al., 2018)

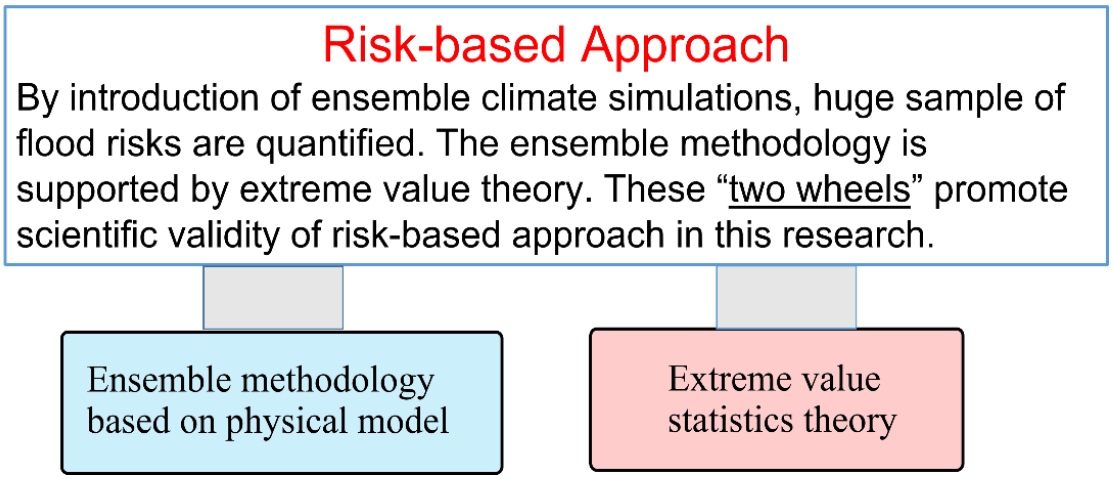

2 Risk-Based Approach for Future Flood Management with Huge Ensembles of Climate Projections in Japan

2.1 Flood risk assessment and social movement in Japan

This chapter explains the latest climate change projection data and risk assessment methods in Japan and concept of the role of ensemble climate data in risk assessment under climate change conditions.

In August 2016, three typhoons landed in the Hokkaido region, Japan, within a week. Typhoon No. 10 approached this region after the landing of these typhoons. These typhoons caused record-breaking rainfall in many parts of Hokkaido, resulting in river flooding, landslides, road and bridge washouts, and extensive damage to land devoted to agriculture, which is the main economic activity in the region (Ministry of Land, Infrastructure and Transport (MLIT), 2017). The members of the Japanese side in this joint research project conducted large-scale climate simulations using a regional climate model under the past and warmer climate condition by using the domestic supercomputer (earth simulator) to develop a 5-km spatial resolution large ensemble climate dataset (e.g., Yamada et al., 2018, Yamada, 2019, Hoshino et al., 2020). The advantage of using this data is that the probability of occurrence and intensity of possible extreme rainfall events can be estimated for each river basin under the past and future climate condition. The annual maximum rainfall and hourly rainfall estimated from the 5-km resolution large ensemble dataset are consistent with observed data for multiple basins in Hokkaido as well as the Chikugo River basin in the Kyushu region and the Tone River basin in the Kanto region, Japan. In addition, the validity of the rainfall volume and occurrence probability of the huge number of simulated heavy rainfalls were demonstrated by a statistical theory (Shimizu et al., 2020).

The ensemble data enables us to estimate flood risk considering rainfall volume and spatio-temporal rainfall patterns. The spatio-temporal rainfall pattern highly affected peak discharge and flood damage for river basins in Japan; however, the rainfall patterns were not considered sufficiently because the experienced rainfall events were limited. On the other hand, ensemble data included many rainfall patterns both similar to experienced and not experienced rainfall patterns.

The flood inundation damage were estimated by using the thousands of rainfall patterns. The flood risk which consists of human and economic damage and probability of occurrence was estimated under past and future climate conditions using the ensemble climate data, hydrological model and flood damage estimation model (Yamada, 2019). This study has contributed to a shift from the traditional hazard-based flood control planning based on past rainfall observations to new risk-based planning for the potential large floods under the future climate. Such detailed risk analysis using ensemble climate data is one of the most advanced efforts worldwide and has been selected as a representative disaster prevention research at the United Nations Framework Convention on Climate Change (UNFCCC Bonn Climate Change Conference) (Yamada, 2019).

From a social point of view, immediately after a series of typhoon tracks in August 2016, the Hokkaido Development Bureau of the Ministry of Land, Infrastructure and Transport (MLIT) and the

Hokkaido Government held an expert committee to review the disaster and consider the risk of unprecedented heavy rainfall and future flooding (MLIT, 2016). The expert's committee summarized that "impacts of climate change should be assessed scientifically, and future flood control measures should be taken based on the risk assessment result". In FY2017, the research group of Hokkaido University conducted a dynamical downscaling to the regional experiment of Database for Policy Decision Making for Future Climate Change (d4PDF) (Mizuta et al., 2017) to develop the dataset of 5-km horizontal resolution (Hoshino et al., 2020). This data is capable of representing highly localized rainfall phenomena, such as topographic rainfall, with high accuracy. In FY2017, climate change impact projection and flood risk were quantified based on the d4PDF with 5-km horizontal resolution. In 2018, the MLIT held meetings to discuss "flood control plans in changing climate" and issued the conclusion in October 2019 (MLIT, 2019). Their analysis using d4PDF estimated that heavy rainfall volume in future climate will be 1.15-fold higher in all of the Hokkaido region relative to heavy rainfall volume under the past climate condition and 1.1-fold higher in all other regions (MLIT, 2019). These evaluations are based on the assumption of reaching a 2 K warmer climate condition compared to pre-industrial climate. Note that global temperatures had already risen by about 1 K at the beginning of the 21st century. In 2019, another committee was held by the Hokkaido Development Bureau of MLIT and the Hokkaido Government and the committee assessed the risk of heavy rainfall and resultant flooding associated with climate change at Tokachi river and Tokoro river basin in Hokkaido, Japan. The committee also considered effective adaptation measures based on the risk assessment. In this technical committee, the rainfall data made by the climate model were considered as "physically possible rainfall data, so-called quasi-observation data."

2.2 Concept of risk-based approach using ensemble climate data

The detailed contents and importance of the risk-based approach with huge ensembles of climate projections in Japan are following. Current flood control plans in Japan are based on projected future rainfall (e.g., 100-year return period), which is derived deterministically from observed rainfall data over the past several decades after the consideration process of rejecting outliers. However, a single data set from the past few decades is only a partial representation of possible rainfall phenomena, given the variability of the climate system. In other words, even if a steady-state is assumed, there is always a range of uncertainties that depend on the timescale. Using an ensemble approach with d4PDF, we were able to assess the uncertainty such as T-year rainfall on a given timescale with a confidence interval, which concept is introduced in chapter 3. Precisely, it equals the realization of uncertainty evaluation considering the degree of freedom of the climate system. Meteorological phenomena occur at different frequencies governed by arbitrary boundary conditions, and the primary boundary condition for the climate system is sea surface temperature (SST). Past experiments of d4PDF used ensemble calculations with multiple initial conditions, including perturbations. The climate model developed by the Meteorological Research Institute (MRI), Japan were used with observed SSTs as the bottom boundary condition. Past climate data are available for a total of 3000-years, including 50 initial perturbations over a 60-year period. In addition, the ensemble climate simulation were also applied for future climate conditions based on global mean temperatures rising between 2–4 K relative to the pre-industrial period. This climate experiment used the six SST patterns from the global-scale coupled atmospheric-oceanic models (two of which are from Japan) which registered in the Fifth Coupled Model Intercomparison Project (CMIP5). The ensemble data for these six models are generated from multiple initial conditions with perturbations. The d4PDF covers the global scale with a spatial resolution of 60 km and the East Asia region with a spatial resolution of 20 km.

One of the risk assessment results is shown following. Figure 2 indicates the risk of potential flooding based on a probability assessment using data from a past experiment, a 2K warmer experiment, and a 4K warmer experiment. Rainfall patterns of all ensemble members (past: 3000 events; 2K warmer: 3240 events; 4K warmer: 5400 events) were inputted to the runoff model, one-dimensional unsteady river flow model, levee breach model, and two-dimensional inundation model. This information allows us to quantitatively discuss the risk of flood damage in the future. Furthermore, fatalities can be estimated from thousands of rainfall events based on the inundation depth, flow velocity, and rate of water level rise. Also, a time development of a F-N curve representing the relationship between the number of fatalities and its occurrence probability is shown in Figure 3. By extending this F-N curve to the time axis, it may be used for discussing future adaptation measures such as advancements in hardware and software measures (Figure 3). Also, other types of regional risk related to major infrastructure facilities and rates of soil runoff have been evaluated using this risk-based approach. In the relevant local communities, discussions regarding these risks have been started.

There are two major advantages of using ensemble information in assessing flood risk under climate change. First, the data enables us to evaluate the range of uncertainty in observed or predicted rainfall and to allow consideration of the degree of freedom in the climate system. By applying this data to past climates and future climates, it is possible to assess the implications for future flooding risks. Another advantage is the ability to assess flooding risk based on the spatiotemporal pattern of projected rainfall. Ensemble data include spatiotemporal distributions of rainfall, which have profound effects on the extent of flood damage and are therefore important to consider when assessing flood risk. This is also essential when developing countermeasures to flooding because it enables the prediction for other potential damage. Thus, the introduction of large ensemble data sets adds a new perspective to flood risk assessment. It will improve decision-making processes. The abovementioned risk-based approach in Japan combines deterministic information from past observations with probabilistic information from ensemble data. The essence of the idea originates from a debate between Einstein and Bohr.

Figure 2 Occurrence probability of overflow and levee failure in per year for past experiments, and 4K warmer experiments (4K future experiment) (inundation depth: 3.2 m) (Yamada, 2020)

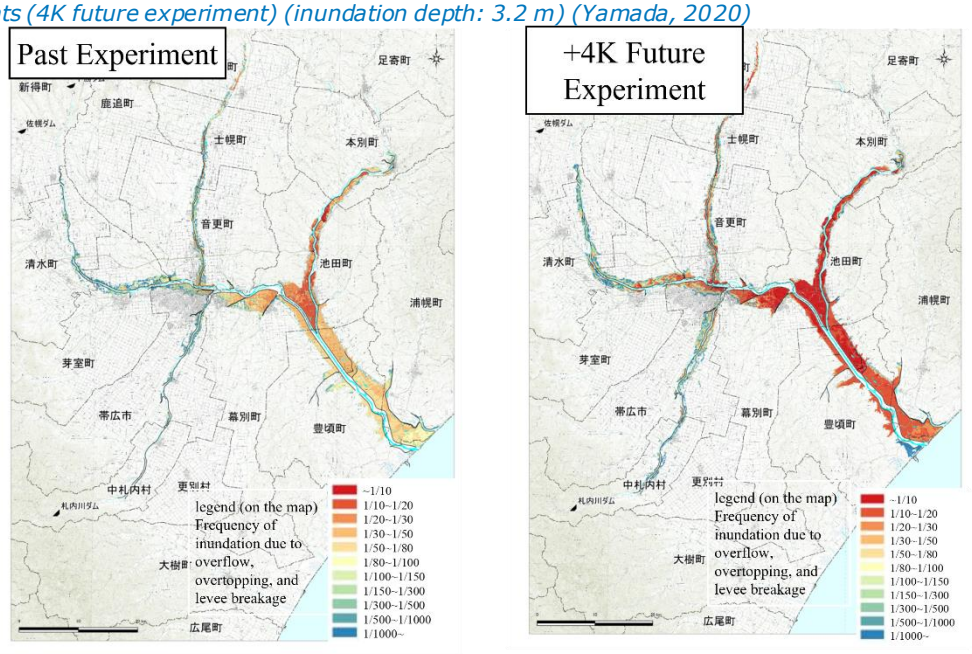

Figure 3 F-N curve on the time axis. The magnitude and shape of the F-N curve are determined by rainfall increment associated with climate change, various adaptive measures, and other factors. (Yamada, 2020)

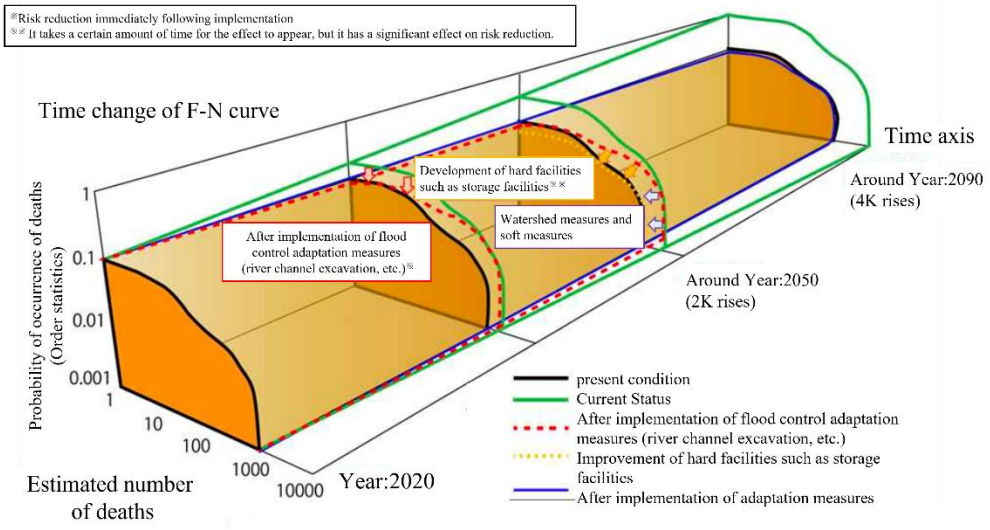

3 Data and Methodology

3.1 Large ensemble climate data

In recent years, a large-ensemble climate simulation database (d4PDF) (Mizuta et al., 2017) has been created and utilized by the research project of the Ministry of Education, Culture, Sports, Science, Japan (SOUSEI, TOUGOU, SI-CAT, DIAS) and Japan Agency for Marine-Earth Science and Technology (JAMSTEC) Earth Simulator Special Promotion Projects. Using d4PDF and its extensive data on past, current, and future climate, it is possible to assess the frequency of extreme weather phenomena that leads to disasters. The d4PDF consists of simulations based on the atmospheric general circulation model (AGCM) called the Meteorological Research Institute AGCM, version 3.2 (MRI-AGCM3.2) (Mizuta et al., 2012) with a horizontal resolution of approximately 60 km (d4PDF-60km), and dynamical downscaling (DDS) from d4PDF-60km to a horizontal resolution of 20 km using the regional climate model (RCM) targeted over east Asia, included Japan (d4PDF-20km). The experimental settings of d4PDF consist of a past climatic condition (past experiment; 50 ensembles×60 years (1951-2010)) and a 4 ℃ warmer climatic condition (4K warmer experiment; six sea surface temperature patterns×15 ensembles×60 years), which has a 4 ℃ warmer global mean air temperature than the pre-industrial period. The sea surface temperature (SST) used in the past experiment was obtained from the Centennial Observation-Based Estimates of SST, version 2 (COBE-SST2) (Hirahara et al., 2014). Small perturbations based on SST analysis errors were added to the initial conditions of the SST to make the ensemble members. The SST used in the +4K experiment consisted of six patterns based on RCP8.5, conducted under phase 5 of the CMIP5 (Taylor et al., 2012). The details of the experimental settings of the d4PDF are presented in Mizuta et al.(2017). Moreover, dynamical downscaling (DDS) was applied to convert annual maximum rainfall events from d4PDF-20km to a horizontal resolution of 5 km (Yamada et al., 2018). The target rainfall event was defined as an event in d4PDF-20km for each year of d4PDF-20km, between June 1 and December 1, where rainfall amounts reached the maximum value in 72-hour over the Tokachi river basin (upper reach of the Obihiro reference point). This study defined the rainfall events as annual maximum rainfall events. For DDS, we employed the NHRCM (Sasaki, 2008), which was used to make the d4PDF-20km. We set the target area of the DDS to 800 x 800 km around Hokkaido. Figure-4 shows the process of dynamical downscaling. Furthermore, we set the number of calculation grids to 161 x 161 in the horizontal direction and 50 in the vertical direction. The Kain-Fritsch convective parameterization scheme (Kain et al., 1993) was used for the DDS. The other physical schemes, such as microphysics, land surface, and boundary layer schemes, were the same as those used in Kawase et al. (2018). The grid-mean topography was used in this study, while Kawase et al. (2018) used envelope-type mountains. This study utilized values from the d4PDF-20km to set the initial and boundary conditions for the calculation. The target period for the DDS was set to 15 days, including the annual maximum rainfall events extracted from the d4PDF-20km. The DDS was performed for a total of 3000 events for the past experiment and 5400 events for the +4K experiment.

Figure 4 Process of the downscaling calculation to make d4PDF-5km (e.g., Yamada et al., 2018)

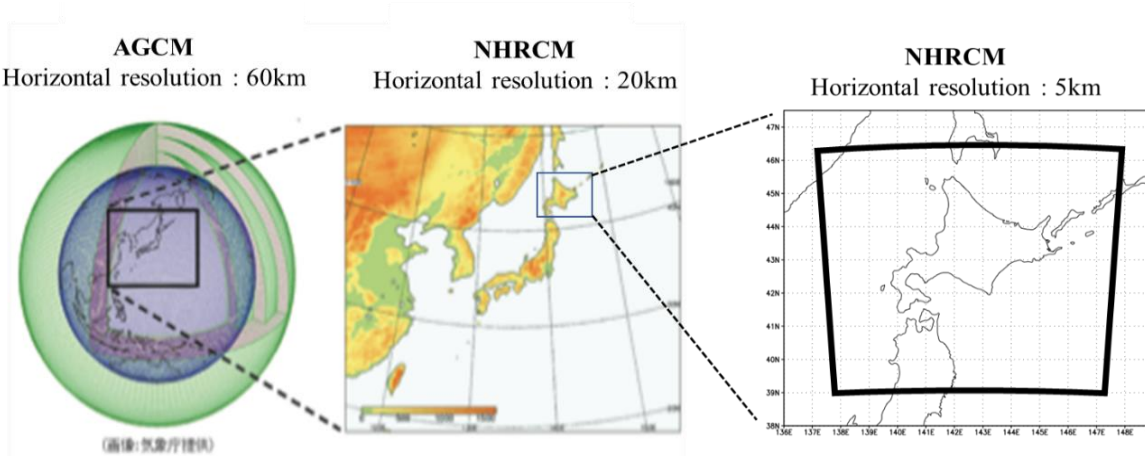

3.2 Estimation method for peak-discharge distribution for each return period

The estimation method for the peak-discharge frequency for each return period consists of three steps, as shown in Figure-5. The first step is the estimation of the rainfall volume frequency for each return period using ensemble climate datasets with the resampling technique. By using this process, the frequency distribution of rainfall with an arbitrary return period, which is a range of arbitrary probability distributions, is defined as a confidence interval. Specifically, the confidence interval includes the population parameter θ with a probability of $(1 - p)$, the interval [L C.I.(X), U C.I.(X)] is constructed with an upper confidence limit value and a lower confidence limit value based on available data. Here, p is the significance level $(0 < p < 1)$. Interval (L C.I.(X), U C.I.(X)] is defined as the $100(1 - p)\%$ confidence interval. The second step is the estimation of the relationship between rainfall volume and peak discharge using the rainfall-runoff model. Rainfall-runoff simulations for several rainfall patterns included in the ensemble climate dataset were conducted to calculate the peak discharges at target points. Next, quantile regression was applied to the relationship between rainfall volume and peak discharge to obtain the relative frequency of peak discharge as a function of rainfall volume. The third step is the estimation of the peak-discharge frequency for each return period. The occurrence frequency of the peak-discharge caused by a given rainfall amount corresponds to the conditional distribution. Therefore, by taking a weighted average of the conditional distribution of peak discharge with T-year rainfall distribution, we derived the probability distribution of the T-year peak discharge.

Figure 5 Estimation method for peak-discharge frequency for each return period

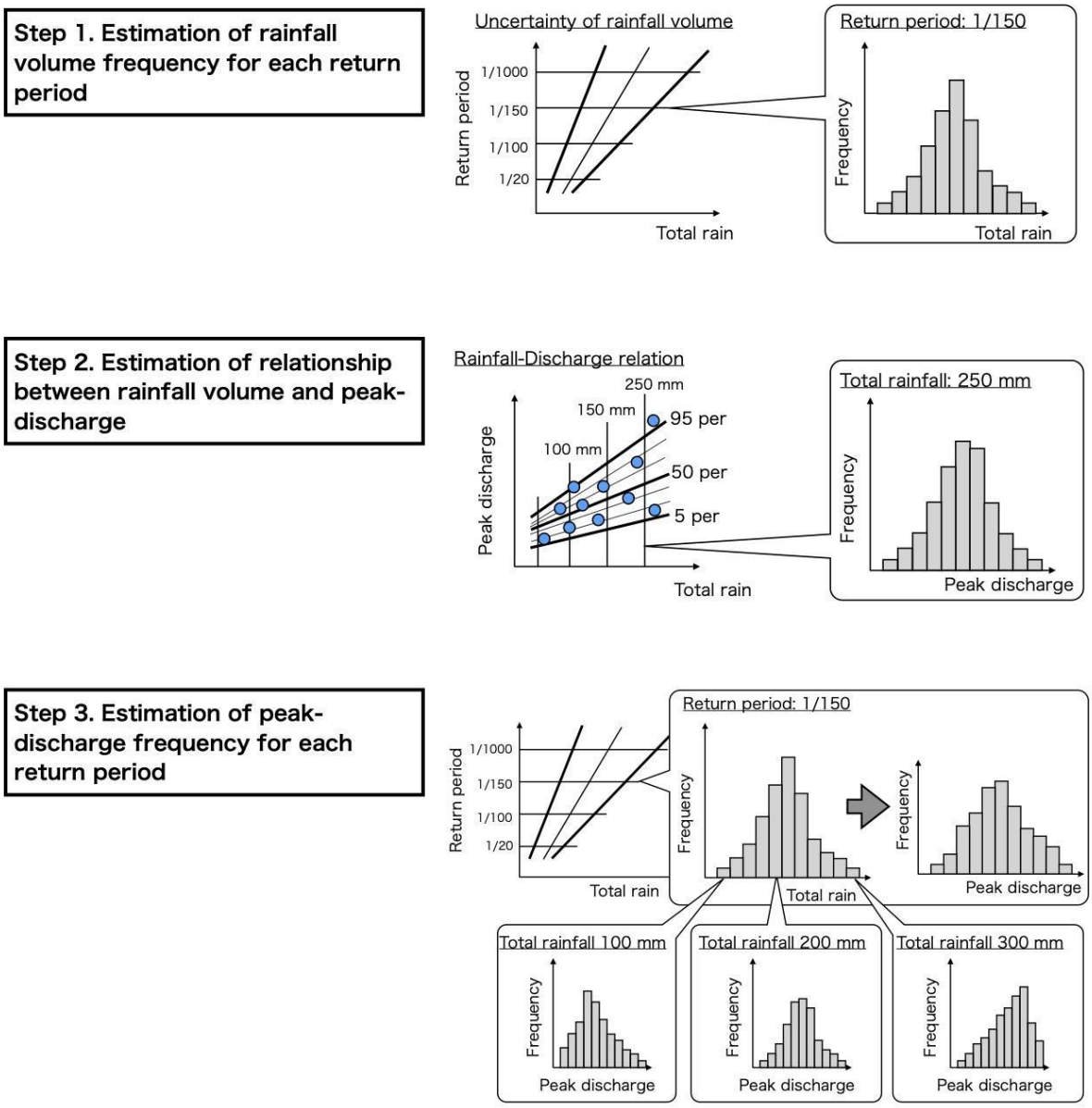

3.2.1 Return period of rainfall

The design rainfall in the current flood control management of Japan is generally calculated by the following steps. First, the observed annual maximum rainfall was fitted to some probability distributions, which are candidates for the estimation of design rainfall. Then, a probability distribution that has the highest level of stability and goodness of fit is adopted. The design rainfall is then obtained as a quantile value corresponding to the target annual exceedance probability "p" in this adopted distribution. A probable rainfall corresponding to exceedance probability "p" means that the occurrence probability of rainfall that exceeds this probable rainfall in a year becomes "p." In addition, the return period is defined as the reverse inverse number of exceedance probability in

an adopted probability distribution. It is an important index in flood control management. Flood control management of the main river basins in Japan adopted a return period of 100–200 years as the design level.

However, the observation period of hydrological quantity in major river basins of developed countries ranges from a few decades to more than a hundred years. This shows that the observation period is shorter than the design return period of the flood prevention facilities. In other words, when using the annual maximum data, the number of observed extremes ranges from a few dozen to a few hundred at most, so that the estimation of the design external force in the conventional hydrological frequency analysis contains uncertainty (estimation error). Because ensemble climate data provide many samples of rainfall based on dynamical models that verify the physical feasibility of the calculated meteorological phenomenon, the uncertainty of the probable rainfall can be quantified as a frequency distribution. In this study, resampling of the ensemble data was conducted to quantify the uncertainty of rainfall for each return period.
The data in d4PDF-5km was resampled to clarify the frequency distribution of the T-year rainfall amount. The d4PDF past experiment is the output of a climate model in which the boundary conditions are the observed SSTs from 1951 to 2010. For this purpose, one annual maximum 72-hour rainfall value from the 50 ensemble members in 1951, and one annual maximum rainfall value from the 50 ensemble members in 1952, were repeatedly extracted until 2010. The annual maximum 72-hour rainfall values for the 60 years from 1951 to 2010 were defined as one sample. In addition, six different SSTs were used in the +4K warmer experiment. In this study, the probability of occurrence of each SST was assumed to be equivalent, and the annual maximum 72-hour rainfall for 60 years was defined as one sample, by extracting one annual maximum rainfall from 90 ensemble members for each year from 2051 to 2110. By applying the aforementioned resampling method, 100,000 samples were generated for both climate experiments. The Gumbel distribution was fitted to each of the 100,000 resampled samples from the past experiment and the +4K warmer experiment to derive the frequency distribution of the T-year probable rainfall. In other words, we estimated 100,000 Gumbel distributions fitted to the annual maximum 72-hour rainfall for 60 years, which yielded 100,000 sets of T-year probable rainfall for a given return period and enabled the estimation of its frequency distribution. Because of the use of the climate model, the introduced resampling method can be interpreted as a physical Monte Carlo method. The cumulative distribution function of the Gumbel distribution is shown in Equation (1).

$$F_X(x) = \exp\left[-\exp\left\{-\left(\frac{x-\mu}{\sigma}\right)\right\}\right] \quad (1)$$

where FX(x) is the cumulative density distribution of the Gumbel distribution, x is the annual maximum rainfall, μ is the location parameter, and σ is the scale parameter.

3.2.2 Rainfall-peak discharge relation

In this study, the frequency distributions of peak discharge as a function of rainfall volume were estimated using quantile regression. The peak discharges have a range even if the rainfall volume is the same because of its spatiotemporal pattern. The relationship between rainfall volume and peak discharge is represented by the following function. The peak discharge range was quantified as percentile values using quantile regression, and each quantile value from the 1st to 99th percentile was extracted for each rainfall volume. The obtained 99 discharges were used to determine the frequency distribution of the peak discharge. By applying quantile regression, the

conditional probability distribution of the peak discharge caused by an arbitrary amount of rainfall can be calculated.

3.2.3 Return period of peak discharge

The frequency distributions of peak discharge for each return period were estimated through the following process. The frequency distribution of rainfall volume for each return period obtained in step 1 (Figure-5), and the frequency distribution of the peak discharge under each rainfall volume obtained in step 2 are used to calculate the frequency distribution of the peak discharge for each return period. Step 3 shows that each bin (section in the histogram) of the rainfall volume has a frequency distribution of peak discharge. The frequency distribution of the peak discharge is expressed by Equation (2).

$$f_{Q_p}\left(q_p,T\right)=\int_r f_{Q_p}\left(q_p \mid r,T\right) f_R\left(r,T\right)dr \qquad (2)$$

where T is the target return period based on rainfall amount, Qp is the peak discharge, R is the rainfall volume, fQp(qp|r,T) is the conditional probability density function of the peak discharge that can occur under a given rainfall volume r, fR(r, T) is the probability density function of T-year rainfall amount, and fQp(qp) is the probability density distribution of the peak discharge.

In this study, the Gumbel distribution was fitted to a set of probable rainfall values derived from the afore-described resampling method to construct a continuous distribution of a probable rainfall fR(r,T) for any given return period T. The Gumbel distribution was also applied to a set of calculated peak-discharge values obtained for a given total rainfall value r, which can be derived from the relationship between the total rainfall in an arbitrary period and the calculated peak discharge, to construct the conditional distribution of peak discharge, fQp(qp|r,T). Equation (2) expresses the probability distribution of the peak discharge fQp(qp,T) under the total rainfall for a given return period T as fR(r,T). Here, fQp(qp,T) is the weighted average of the conditional distribution of peak discharge under a given rainfall value fQp(qp|r), where the distribution of rainfall fR(r,T) is derived from d4PDF-5km.

The afore-described method for the probability peak discharge integrates the conditional distribution (expressed by the relationship between the total rainfall and peak discharge obtained from the rainfall-runoff model) and the distribution of the probable rainfall from the ensemble climate data. In other words, the method is capable of updating the probability distribution of the output peak discharge, as the climate model and rainfall-runoff model differ or become more sophisticated.

3.3 Hydrological model

This section describes the rainfall-runoff models adopted by the two countries in working package 1. The characteristics of rainfall and peak discharge represented by these physical models allow us to evaluate the uncertainty of the model calculation.

3.3.1 wflow_sbm

Wflow_sbm is a conceptual bucket-style hydrologic model based on simplified physical relationships, and it uses a kinematic wave surface and subsurface routing for lateral transport.

The wflow_sbm model is a fully distributed hydrological model that allows the use of high-resolution spatial input data. This makes the model well suited for the use of high-resolution climate model output, as presented in Section 3.1. A schematic of the most relevant vertical and horizontal processes in the wflow_sbm concept is shown in Figure 6.

The wflow_sbm model for the Tokachi River basin was set up based on globally available data at a resolution of approximately 1 × 1 km^2. The river network, river length, and slope parameters were derived from the state-of-the-art hydro-MERIT dataset (Yamazaki et al., 2019). The hydrological parameters for the soil were derived from the GLOBCOVER land cover map and SoilGrids in the 250m soil database. The parameters were derived and scaled to model resolution using point-scale (pedo)transfer functions in combination with multiscale parameter regionalization (MPR) techniques.

Figure 6 Schematic of the wflow_sbm concept showing the vertical and horizontal processes for a specific grid cell (left) and the river network of the wflow_sbm model (right).

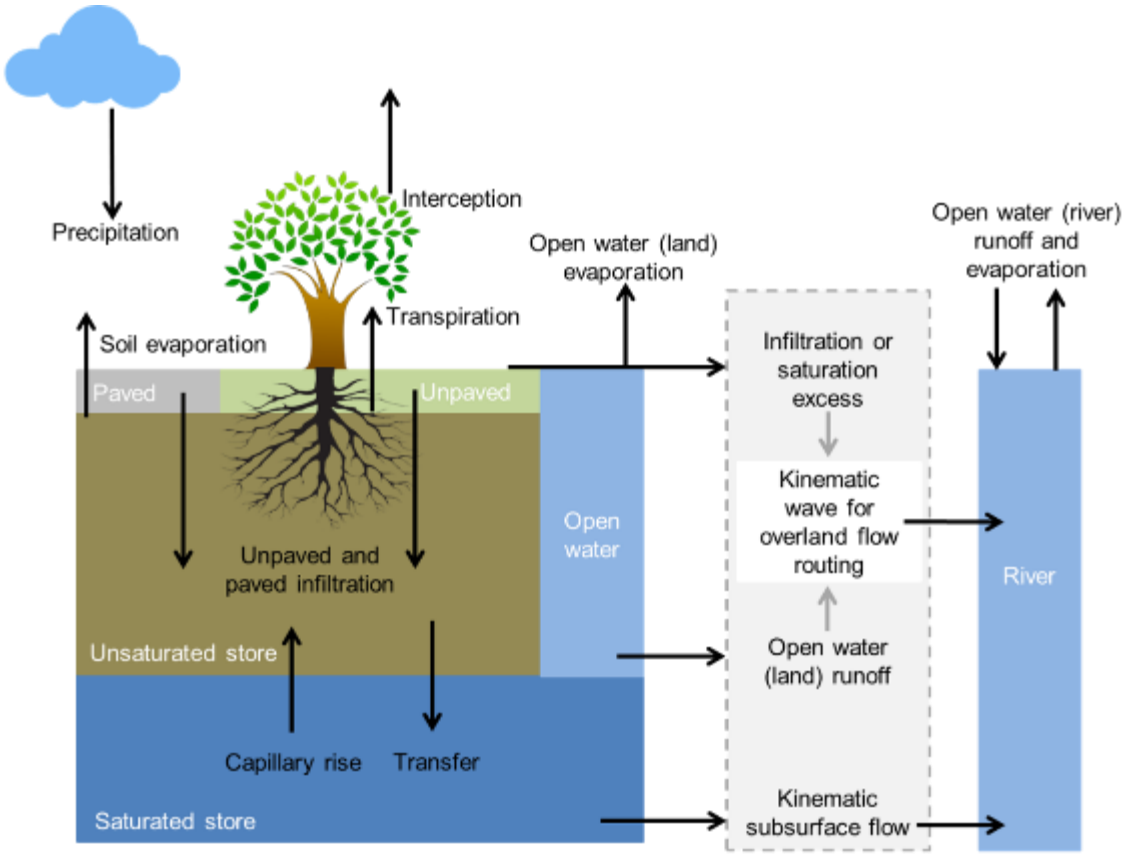

The wflow_sbm model for the Tokachi river basin was set up using globally available data at a ~1x1 km2 model resolution. The river network, river length and slope parameters are derived from hydro-MERIT dataset (Yamazaki et al. (2019)), using the state-of-the-art upscaling techniques to preserve information from the high-resolution base date (Eilander et al., 2021). The hydrological parameters for the soil are derived from the VITO land cover map and the SoilGrids250m soil database. The parameters are derived and scaled to the model resolution using point-scale transfer functions in combination with Multiscale Parameter Regionalization (MPR) techniques (Imhoff et al., 2020).

Figure 7 3D visualization of the wflow model of the Tokachi river basin.

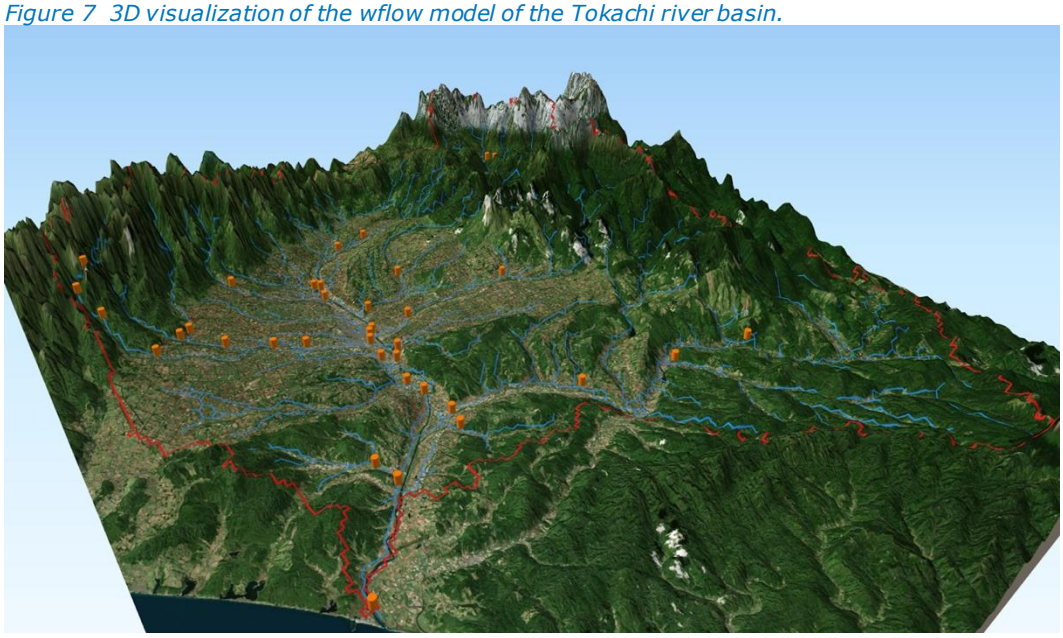

The wflow model is used worldwide to simulate rainfall-runoff processes. The wflow model can be used for event-based modeling, as well as for continuous simulations. For this, an advanced soil water accounting scheme is included in the model. This also makes the model very suited for drought situations. And since the model is physically based, the model can also be used to simulate the effects of climate change on the hydrological response.
All relevant rainfall-runoff processes for flood peak estimation are included in the model. The model includes snow and glacier processes, for cases where rapid snowmelt contributes to the existence of floods, a soil water accounting scheme, and routing of surface and (rapid) subsurface water.

3.3.2 MATSIRO

The Minimal Advanced Treatments of Surface Interaction and Runoff (MATSIRO) (Takata et al., 2003) was also used in this study. MATSIRO can simulate the exchange of water vapor, energy, and momentum between the land surface and atmosphere on a physical basis. The interaction between the atmosphere and land surface can be simulated using this model with a GCM. MATSIRO has been used for various impact assessments of the hydrological cycle, such as the impact of human activities (Pokhrel et al., 2017) and groundwater impacts (Koirala et al., 2014). Recently, a system for estimating the conditions of land surfaces and rivers in real-time has been developed and operated (Today's Earth). This system consists of MATSIRO and the river routing model CaMa-Flood (Yamazaki et al., 2011). Meteorological forecast and observation data were used as input data for the system to estimate the risk of water-related disasters on a global scale.

The schematic diagram of MATSIRO is shown in Figure 8. MATSIRO represents the canopy as a single layer and illustrates the simulation of the energy and heat exchange between the ground surface and the atmosphere. MATSIRO solves the surface and subsurface runoff by considering the following four runoff types: the base flow, saturation excess runoff (Dunne runoff), infiltration excess runoff (Horton runoff), and overflow of the uppermost soil layer. The first three runoff types were calculated by applying a simplified TOPMODEL (Beven and Kirkby, 1979), which assumes a subgrid-scale slope profile. The assumed slope profile was used to estimate the saturation fraction required for the calculation of the first three runoff types.

In this study, we performed offline simulations using MATSIRO, which was decoupled from the GCM. We did not use human activities and groundwater modules of MATSIRO to focus on a simple rainfall-runoff process, same as the other runoff model. The near-surface atmospheric data of d4PDF-5km were used as the boundary condition of MATSIRO to calculate the runoff of each grid point within the target basin. The obtained runoff was fed to the Rainfall-Runoff-Inundation (RRI) model under non-infiltration conditions to calculate the river discharge.

Figure 8 Schematic diagram of MATSIRO. The symbols of the variables are the prognostic variables and heat and vapor fluxes in MATSIRO, which are listed in the right table (Takata et al., 2003).

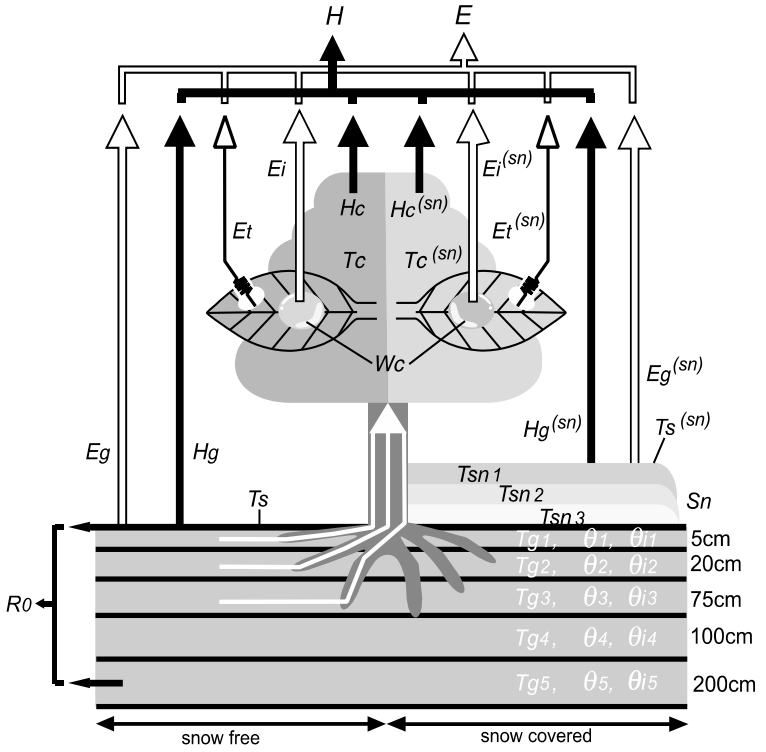

Internal prognostic and diagnostic variables of MATSIRO

Variable	Description	Unit	Array[a]
Prognostic variables			
in LNDFLX[b]			
T_s	surface temperature	K	
T_c	canopy temperature	K	
in LNDSTP			
T_g	soil temperature	K	soil layer (5)
θ	soil moisture (solid + liquid)	m^3/m^3	soil layer (5)
θ_i	frozen soil moisture	m^3/m^3	soil layer (5)
w_c	canopy water	m^3/m^2	–
S_n	snow water equivalent	kg/m^2	–
T_{sn}	snow temperature	K	snow layer (1–3)
α_{sn}	snow albedo	–	V/N/I[c]
Diagnostic variables			
in LNDFLX[b]			
τ_x	zonal wind stress	N/m^2	–
τ_y	meridional wind stress	N/m^2	–
H	sensible heat flux	W/m^2	–
E_i	interception evaporation	$kg/m^2/s$	–
E_t	transpiration	$kg/m^2/s$	–
E_g	ground evaporation	$kg/m^2/s$	–
E_s	sublimation	$kg/m^2/s$	–
R_u	upward radiation	W/m^2	V/N/I[c]; D/R[d]
α_s	surface albedo	–	V/N/I[c]
F_g	surface heat conduction	W/m^2	–
ΔF	surface energy residual	W/m^2	–
in LNDSTP			
A_{Snc}	frozen fraction on canopy	–	–
F_{root}	root uptake	$kg/m^2/s$	soil layer (5)
R_o	runoff	$kg/m^2/s$	–

[a] Numeral in the parenthesis is the number of layers.
[b] Variables in LNDFLX are calculated for the snow-free and the snow-covered potions.
[c] V: visible, N: near infrared, and I: infrared.
[d] D: direct beam, R: diffuse radiation.

3.3.3 RRI model

The RRI model was developed by the International Center for Water Hazard and Risk Management (ICHARM). The RRI model was employed to simulate flood inundation and identify flood-prone areas. The RRI model is a two-dimensional model that is capable of simulating rainfall-runoff and flood inundation simultaneously (Sayama et al., 2012, Sayama et al., 2015). At a grid cell in which a river channel is located, the model assumes that both the slope and river are positioned within the same grid cell. The channel was discretized as a single line along the centerline of the overlying slope grid cell. The flow on the slope grid cells was calculated using the 2D diffusive wave model, whereas the channel flow was calculated using the 1D diffusive wave model. The RRI model simulates the lateral subsurface, vertical infiltration, and surface flows to represent flood characteristics better. The lateral subsurface flow, which is more important in mountainous regions, was treated in terms of the discharge–hydraulic gradient relationship, including both saturated subsurface and surface flows, whereas the vertical infiltration flow was evaluated using the Green–Ampt model. The details of the model are presented below (Sayama et al., 2012). Figure-9 shows the model element in RRI.

Figure 9 Schematic of the RRI model (https://www.pwri.go.jp/icharm/research/rri/index.html)

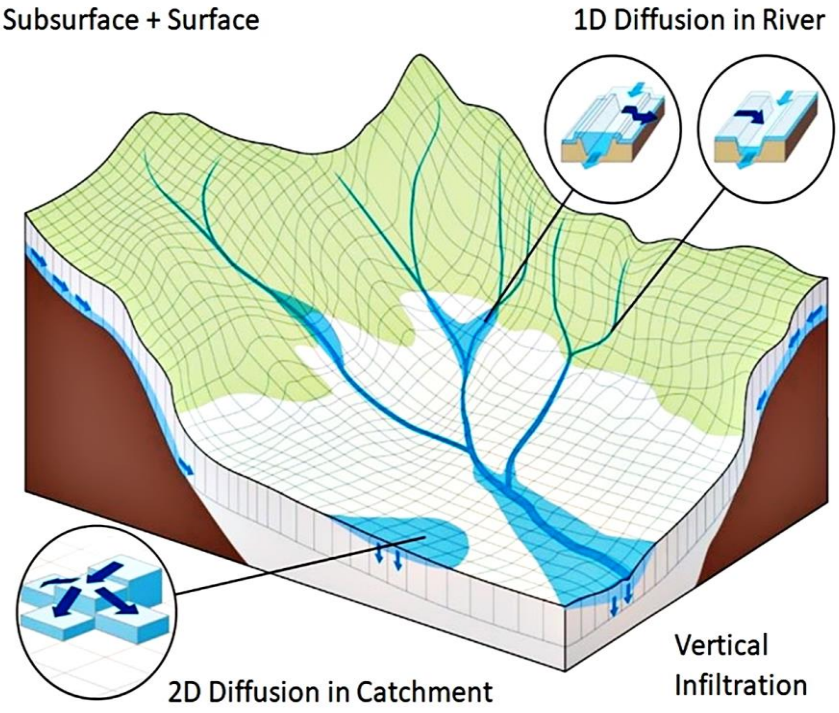

3.4 Runoff simulation of 2016 flood

3.4.1 wflow_sbm

The wflow_sbm model was calibrated for the 2016 event. This event includes 3 consecutive flood peaks within the month of August. The parameters that were used in the calibration are the M-parameter which is linked to the decrease of hydraulic conductivity of the soil with depth, and the KSatHorFrac parameter which is the factor linking the horizontal to the vertical hydraulic conductivity of the soil.
The calibration was done by comparing simulated discharges with observed discharges for the selected event for 4 stations in the basin: The Tokachi dam inflow, the Satsunai dam inflow, the Satsunai point and the Obihiro points. The locations are indicated on the map below.

Figure 10 Overview of the Tokachi catchment and the selected calibration stations.

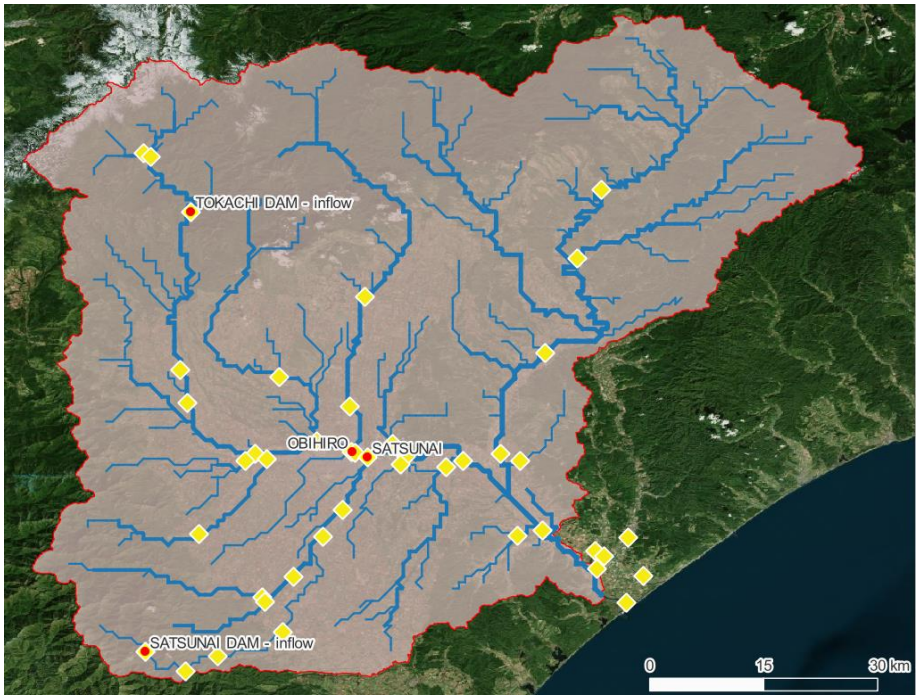

In figure 11, the results of the simulation are shown for different stations in the basin. As can be seen, the model is capable of capturing the discharge at Obihiro reasonably well. The model slightly overestimates the first two peaks, but underestimates the last peak. This might have to do with the rainfall data, or the effect of the dams, which are not well captured in the model yet. It can also be seen that the underestimation is most likely coming from underestimating the flow in the Satsunai river. Especially the inflow into the Tokachi dam is very well simulated, whereas the inflow to the Satsunai dam is largely underestimated. The reason for the underestimation could be that this basin is hydrologically very different, resulting in different parameter values needed to capture the peaks, or, more likely, that the rainfall is underestimated.

Figure 11 Results for the selected parameter set, showing the discharge time series for different observation stations.

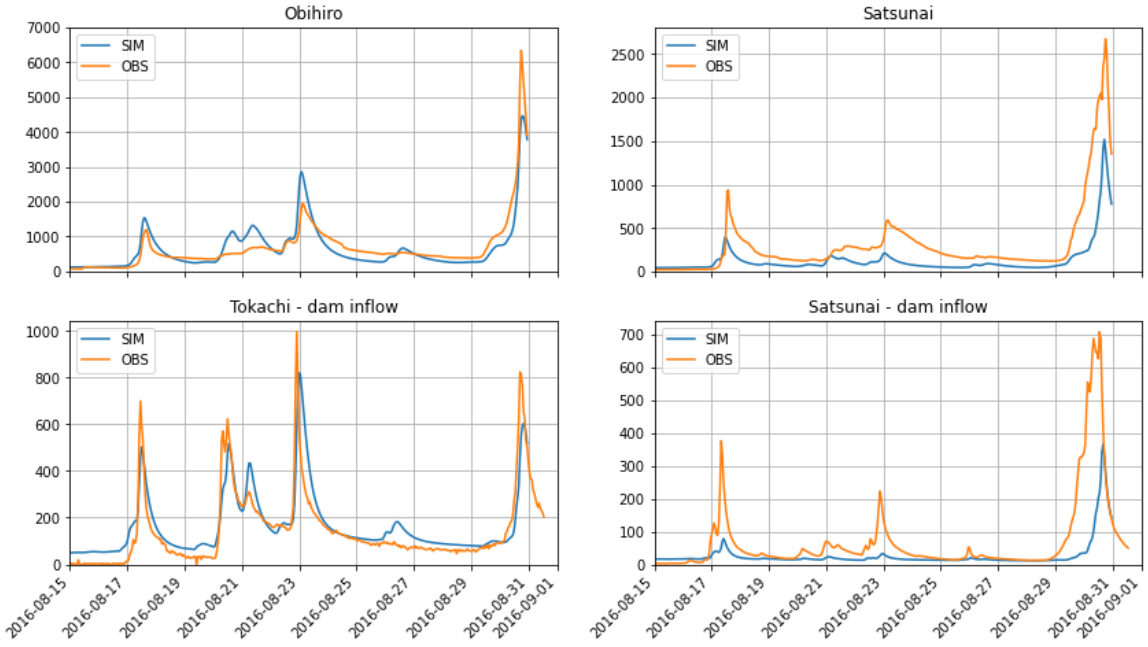

In figure 12 the time series for the cumulative volume are shown. The figures indicate that for Tokachi dam and Obihiro point, the amount of water in the model is in line with observations, but how the discharge is distributed over time, is not always the same. Especially the inflow of the Satsunai reservoir is underestimated. This could be explained by underestimation of the rainfall in the Satsunai basin.

Figure 12 Results for the selected parameter set, showing the cumulative discharge time series for different observation stations.

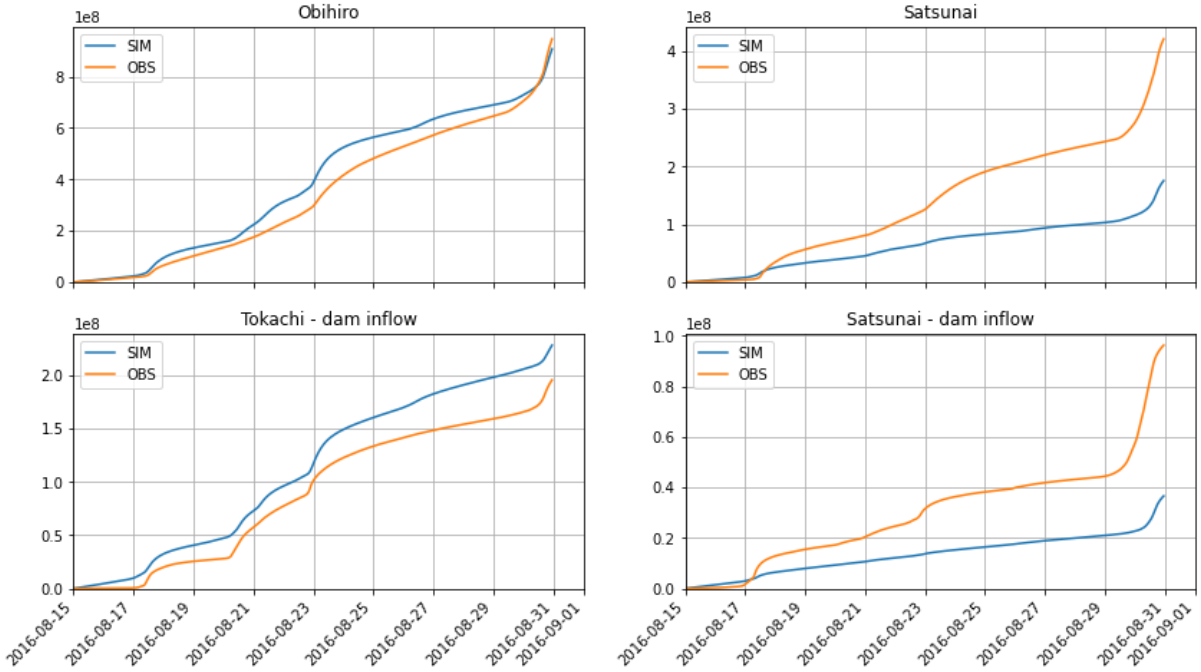

3.4.2 RRI model

The calibration was conducted as targeting the 2016 flood event. The simulations with the four model parameters and three different parameter settings were conducted. The target parameters and conditions of sensitivity analysis are shown in Table 1. Finally, three land cover types were set up for the target basin, and parameters were set for each land cover type.

Table 1 Parameter setting for sensitivity analysis

Manning's roughness parameter for river ($m^{-1/3}/s$)	0.02	0.03	0.04
Manning's roughness parameter for slope ($m^{-1/3}/s$)	0.3	0.4	0.5
Soil depth (m)	0.5	1.0	1.5
Lateral saturated hydraulic conductivity (m/s)	0.05	0.10	0.15

Figure13 Result of sensitivity analysis of inflow to the Tokachi dam (Influence of (a) Manning's roughness on river cells, (b) Manning's roughness on slope channel, (c) Soil depth and (d) Lateral saturated hydraulic conductivity)

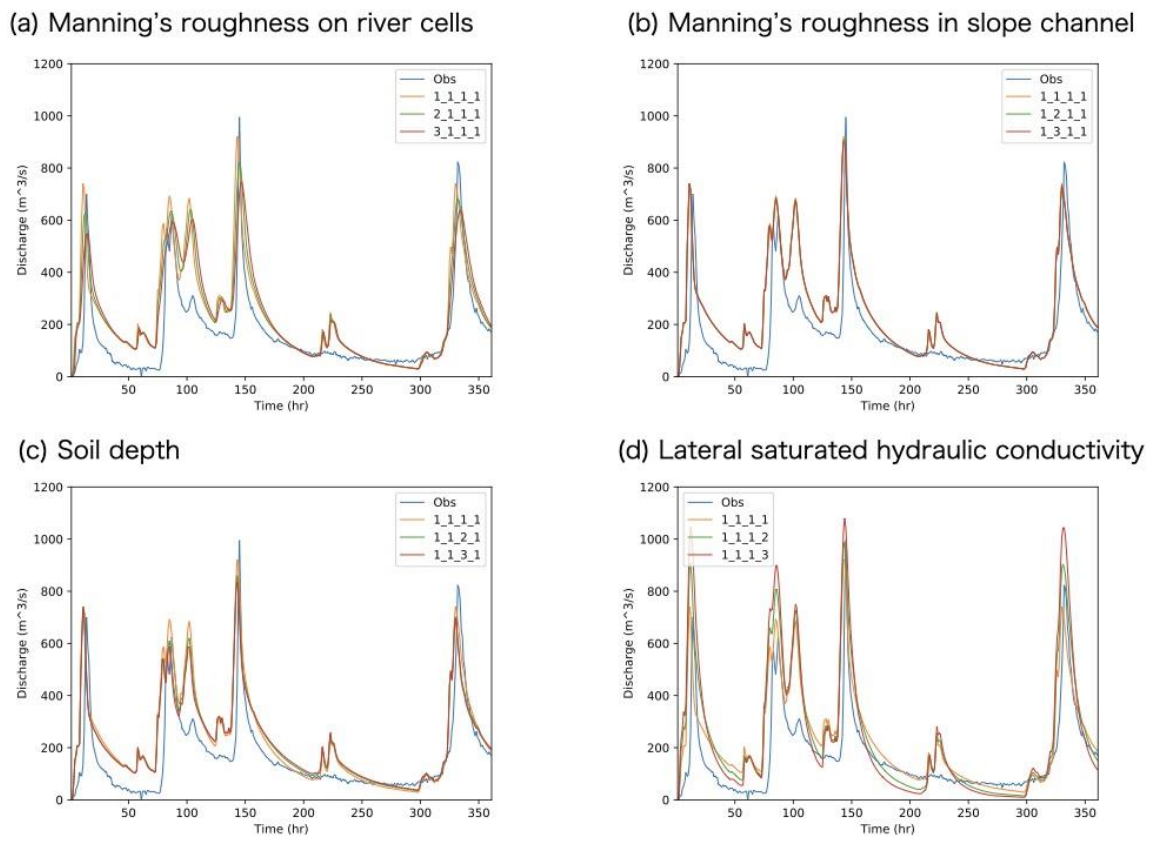

4 Results

4.1 Probability distribution of Rainfall with target return period

Figure 14 shows the confidence intervals of the probable rainfall in the Tokachi River basin for the past experiment and the +4K warmer experiment. In this figure, the black dots represent the observed annual maximum basin-averaged 72-hour rainfall, and the solid blue line is the Gumbel distribution that these observations are assumed to follow. In addition, the blue and red areas represent the confidence intervals of the probable rainfall for the past and future climates, respectively. The confidence intervals for past and future climates were constructed using the physical Monte Carlo method described in Section 3.2.1. The number of calculated annual maximum rainfall in each resampled sample is described in Section 3.2.1. was the same as the observation. The existence of the purple overlap area between the two intervals indicates that heavy rainfall events with the same return period, but with different frequencies, can physically occur in both climates, where the global average temperature differs by 4 K. The results of the probability assessment based on ensemble climate data were also supported by statistical theory, and research results were obtained to ensure scientific validity (Shimizu et al., 2020). In this study, we adopted the probability limit method (Moriguti, 1995), which allows us to derive the statistical threshold of rainfall that can occur under the assumed probability distribution of annual maximum rainfall, and constructed confidence intervals based on this test. The blue and red dotted lines in Figure 14 show the width of the confidence interval based on this theory. The figure shows that the confidence intervals based on the ensemble climate data and the confidence intervals based on the probability limit method coincide very well for both past and future climates. The coincidence of the confidence intervals constructed independently from the physical Monte Carlo calculations, and the probability limit method supports the mathematical validity of the present study.

Figure14 Confidence interval of probable rainfall derived from d4PDF-5km (Shimizu et al., 2020)

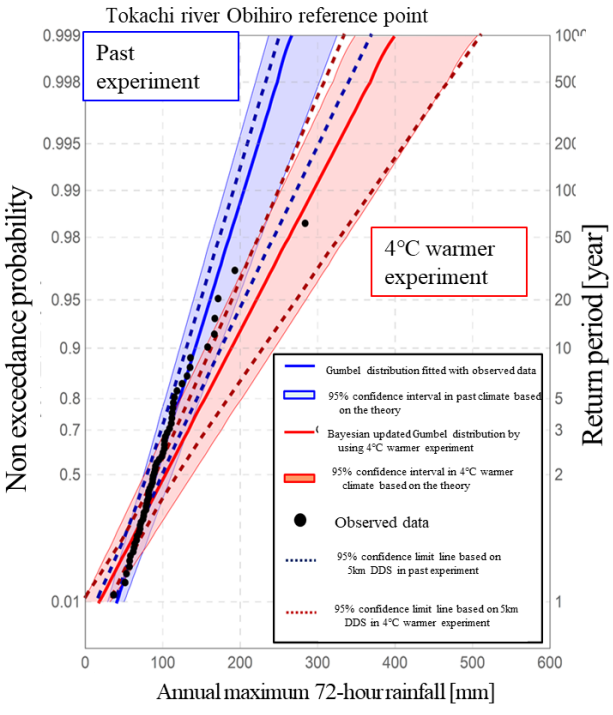

In this study, the Gumbel distribution was fitted to the frequency distribution of the annual maximum 72-hour rainfall in a given return period, derived from d4PDF-5km. A 150-year return period was used as an example, and the probability density function of the Gumbel distribution for the past and 4K warmer experiment is shown in Figure 15. From this figure, Gumbel distribution fitted well with the frequency distribution of 150-year annual maximum rainfall derived from d4PDF-5km. By functionalizing the probable rainfall distribution with a continuous distribution, the probability distribution of the T-year peak discharge, which is discussed in the next section, can be calculated analytically.

Figure 15(a) Frequency distribution of 150-year annual maximum 72-hour rainfall in past experiments (blue bins) and the probability density function f R(r,150) of the Gumbel distribution fitted to the frequency distribution (solid blue line)

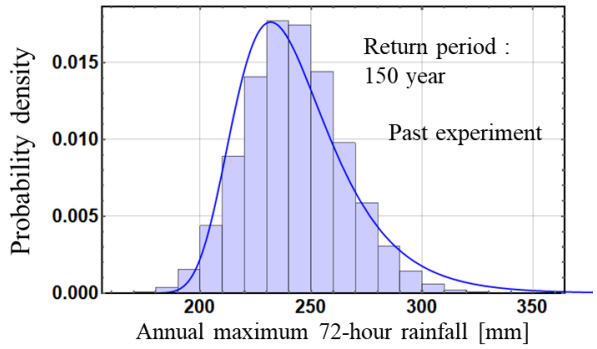

Figure 15(b) Frequency distribution of 150-year annual maximum 72-hour rainfall in 4K warmer experiments (red bins) and the probability density function f R(r,150) of the Gumbel distribution fitted to the frequency distribution (solid red line).

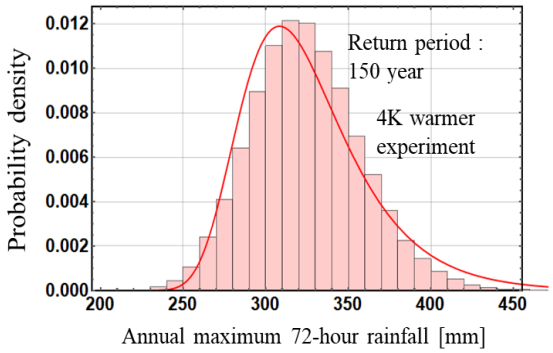

4.2 Rainfall-Peak discharge relation

In this section, a method for calculating the relationship between total rainfall and associated peak discharge is presented. Figure 16 shows the relationship between peak discharge in the river and the annual maximum 72-hr rainfall over the Tokachi River Obihiro reference point basin. The large circles in the figure represent observed results; the small circles are the results from past experiments (blue) and 4K warmer experiments (red). The peak discharges in both experiments were obtained through the runoff and channel routing models used for river planning in the same basin. In Figure 16, the observed data show that peak discharge increases with increasing mean basin rainfall, which is also confirmed by the results of past experiments.

Furthermore, in the 4K warmer experiment, the same trend in peak discharge occurs while covering a larger range of rainfall. Given that the same runoff parameters are used in this study, it is evident that the difference in peak discharge for the same amount of rainfall depends on the spatiotemporal distribution of that rainfall. Incidentally, the maximum observed value was during the flooding and landslide disaster in August 2016, suggesting that these rainfall events significantly raised the peak discharge. A similar analytical approach may be applied to river basins throughout Japan, which will allow us to discuss the importance of spatiotemporal variation in rainfall and its influence on peak flow.

In this study, the quantile regression curve was fitted to the relationship between the annual maximum 72-hour rainfall and the peak discharge in each experiment, and the extrapolation of the peak discharge was calculated for a given annual maximum 72-hour rainfall. The quantile regression curve used is shown in Equation (6). The relationship between the annual maximum 72-hour rainfall and the peak discharge for each experiment and the estimated quantile regression curves are shown in Figure 18(a,b). The conditional frequency distribution of the peak discharge

that can occur for a given rainfall can be calculated. In this study, the continuous distribution $f_{Qp}(Qp|r,T)$ was calculated by applying the Gumbel distribution to this conditional frequency distribution. Figure 18(a,b) shows the conditional probability density function of the peak discharge for each experiment at a given rainfall value of 300 mm.

$$Q_p = aR^2 + bR \tag{6}$$

where Qp is the peak discharge; R is the annual maximum72hour rainfall; and a and b are parameters of the quantile regression curve. The extreme large discharge events are limited though using the large ensemble climate dataset. However, using the function of the rainfall and peak discharge can cover the area of extreme large discharge. Note that extreme large discharge is sensitive to the formula of the relationship between rainfall volume and peak discharge. For that reason, the type of the formula should be considered based on the characteristics of the target river basin.

The relationship between the rainfall volume and the peak discharge is determined based on spatio-temporal rainfall patterns and differences of runoff models and those parameters. The scatter plots of rainfall volume and peak discharge derived from the integration of described hydrological models in Section 3.3 are shown in Figure 19. Note that the parameter of the runoff models described in 2.3 need to be adjusted for practical use. The target rainfall events of three additional models are the top 50 rainfall volume events from d4PDF (Past) and the top 100 rainfall volume events from d4PDF (+4K). The results of all models show that a wide range of peak discharges can be taken for large rainfall events. The proposed method can estimate peak discharge distribution at each return period in consideration of multiple runoff models by applying the aforementioned regression curve to the rainfall-peak discharge relationship for each runoff model or for the combining result of runoff models. In the following part, the return period of the peak discharge is estimated according to the relationship between rainfall volume and peak discharge of a single model.

Figure16 Relationship between annual maximum 72-hour rainfall and peak discharge at the reference point in the Tokachi River basin

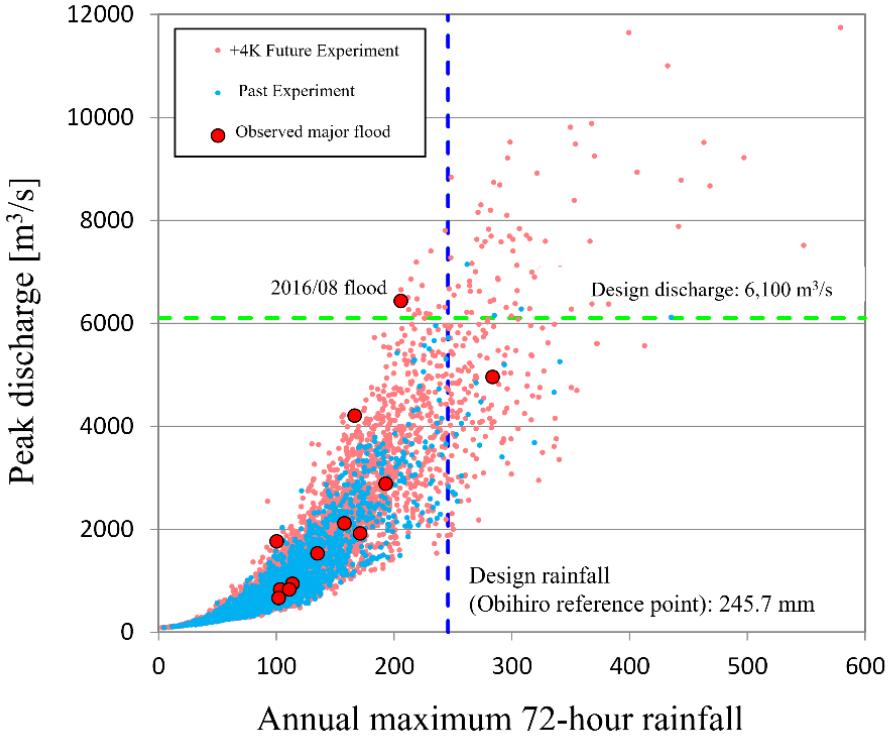

Figure 17(a) Relationship between annual maximum 72-hour rainfall and peak discharge at the same reference point and quantile regression curve in the past experiment.

Figure 17(b) Relationship between annual maximum 72-hour rainfall and peak discharge at the same reference point and quantile regression curve in the 4K warmer experiment

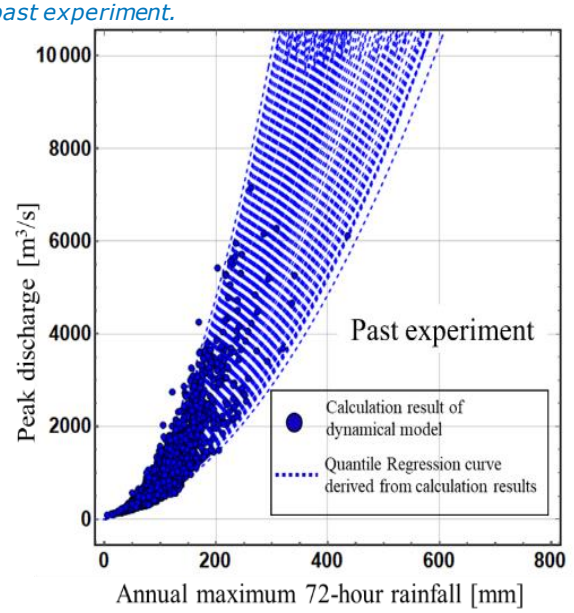

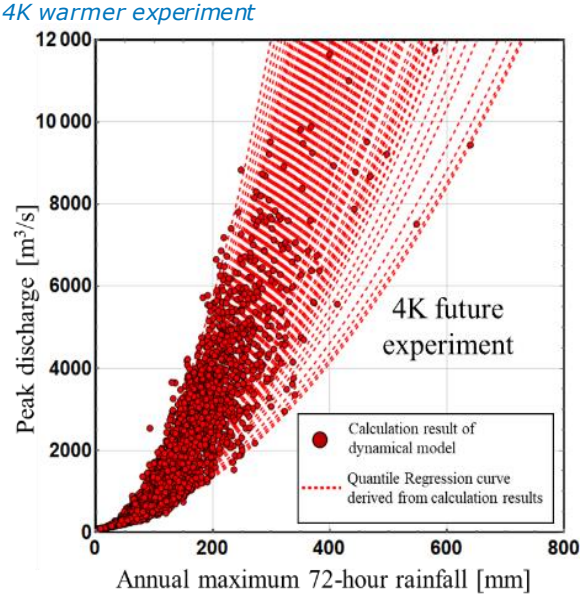

Figure 18(a) Frequency distribution of probable peak discharge (blue bins) and probability density function of the Gumbel distribution f Qp(q p|r=300, 150) fitted to the distribution (solid blue line) when the maximum 72-hour rainfall in a 150-year probability year is 300 mm in the past experiment.

Figure 18(b) Frequency distribution of probable peak discharge(red bins) and probability density function f Qp(q p|r=300, 150) of the Gumbel distribution fitted to the distribution (solid red line) when the maximum 72-hour rainfall value for a 150-year

probability year in the 4K warmer experiment is 300 mm.

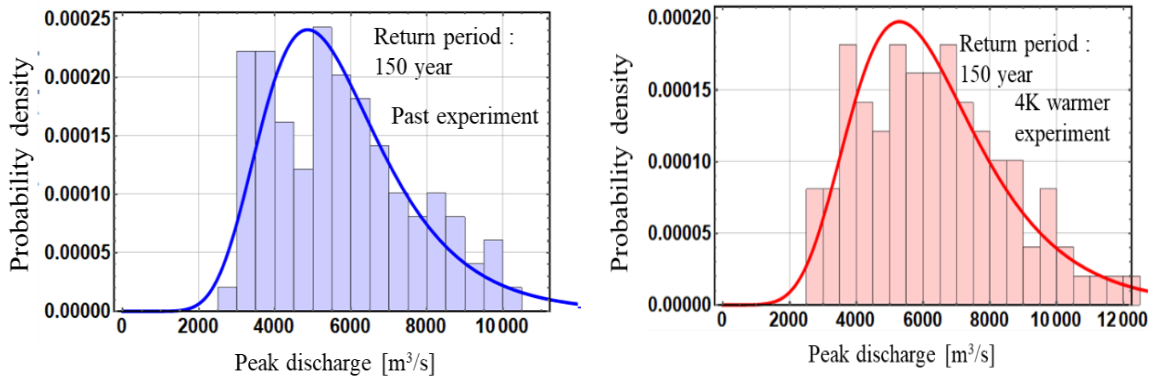

Figure19 Relationship between annual maximum 72-hour rainfall and peak discharge estimated by the different runoff models at the reference point in the Tokachi River basin
※Note that the initial condition and parameters of the RRI, wflow and MATSIRO need to be adjusted for practical use

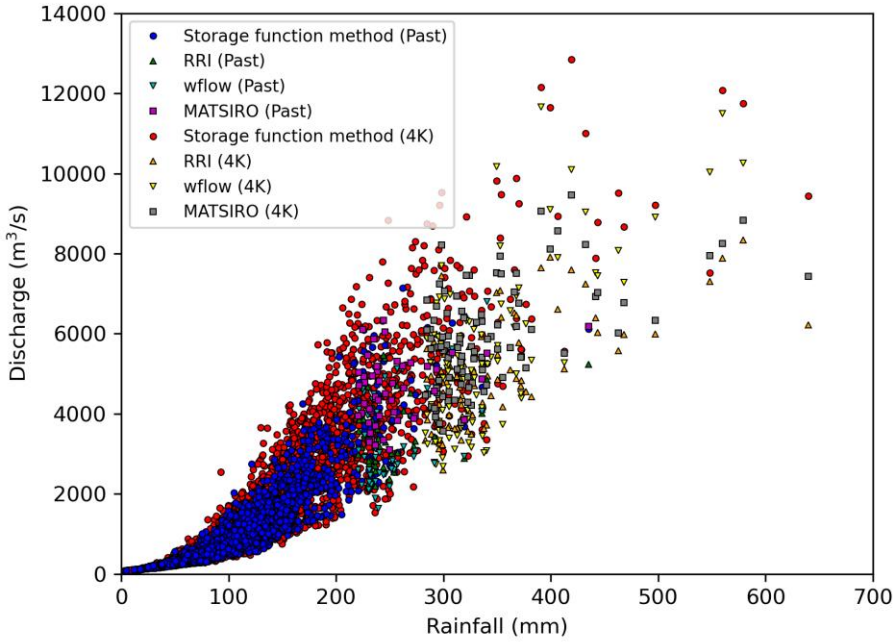

4.3 Peak discharge return period

Figure 20 and Figure 21 show the derivation process of the probability distribution of the 150-year peak discharge in the previous experiment and the +4K warmer experiment. Figure 22 shows a comparison of the probability density function of the 150-year peak discharge for the past experiment and the +4K warmer experiment. It can be observed that the shape of the probability distribution gets shifted under different climatic conditions. The multiplier of future change is 1.88 for the expected value, and 2.04 for the 95% upper confidence limit of the +4K warmer experiment and the past experiment, respectively.

The calculation process is shown in (Figure 20 and Figure 21). By setting the target probability scale T of the design rainfall (150 years in this section), the horizontal axis of the annual maximum peak flow relationship is the 150-year probability rainfall, and the vertical axis is the peak discharge that can occur under the 150-year probable rainfall. The probability distribution of the peak discharge that occurs for a given rainfall r, fQp(qp|r, 150), are weighted and averaged with the 150-year probability annual maximum 72hour rainfall distribution f R(r, 150) to obtain the probability distribution of the 150-year peak discharge fQp(qp, 150). It is evident from both figures that the relationship between the annual maximum 72-hour rainfall and peak discharge increases more in magnitude under the future climate as compared with the past climate, owing to the spatiotemporal concentration of rainfall (Hoshino and Yamada, 2018). Figure 23 shows the relationship between the return period of annual maximum rainfall and peak discharge in both past and future climate conditions. From this diagram, the proposed method enables the estimation of uncertainty in T-year peak discharge.

The 150-year peak discharge based on this method was calculated at the Obihiro, Satsunai, Bisei, and Otohuke River confluence points. These probable peak discharges can be used as a starting point for the evaluation of water levels caused by flows equivalent to the planned probability scale, the evaluation of the probability of overtopping and levee breaching, and the quantification of human and economic risks.

Figure20 Process of deriving the T-year probability peak discharge under the past climate condition

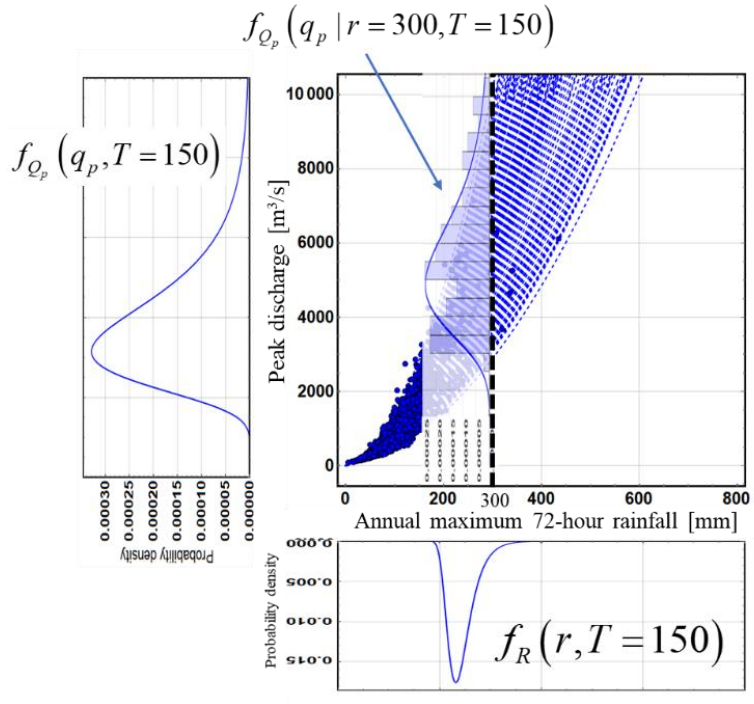

Figure21 Process of deriving the T-year probability peak discharge under the 4K warmer climate condition

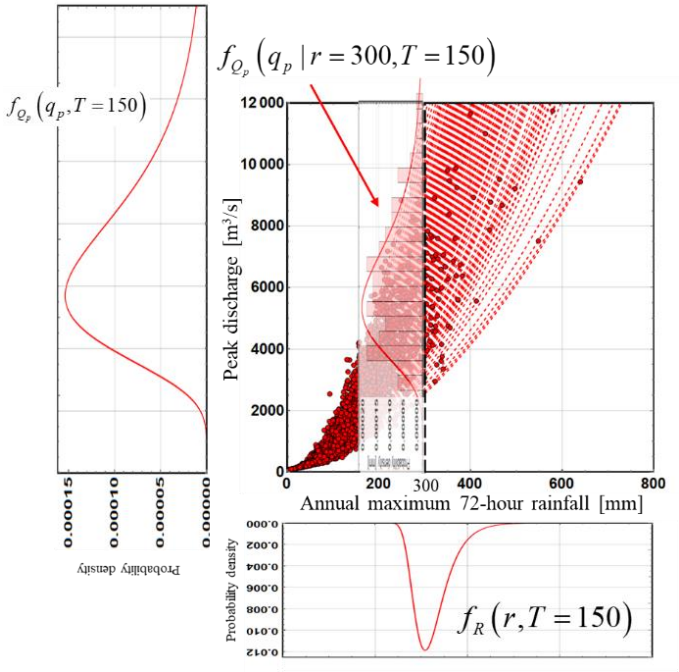

Figure22 Comparison of the probability density function of the 150-year probability peak discharge for the past experiment and the 4K warmer experiment

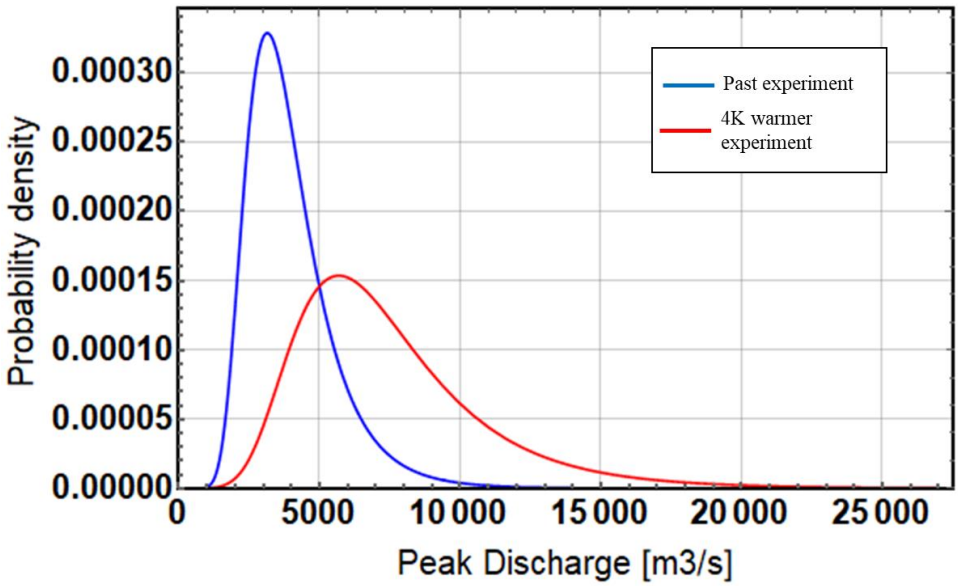

Figure 23(a) Relationship between return period of annual maximum rainfall and peak discharge in past experiment
Blue solid curve; mean value
Blue dotted curve; 95% confidence limit line

Figure 23(b) Relationship between return period of annual maximum rainfall and peak discharge in 4K warmer experiment
Red solid curve; mean value
Red dotted curve; 95% confidence limit line

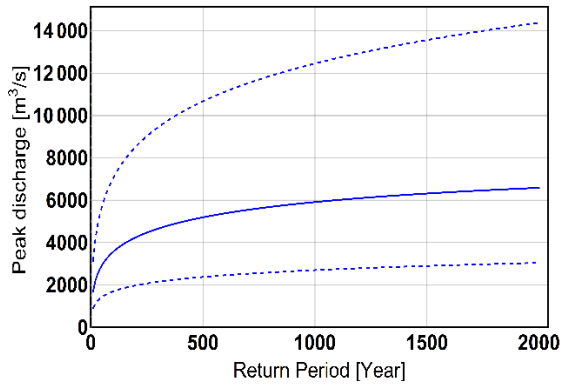

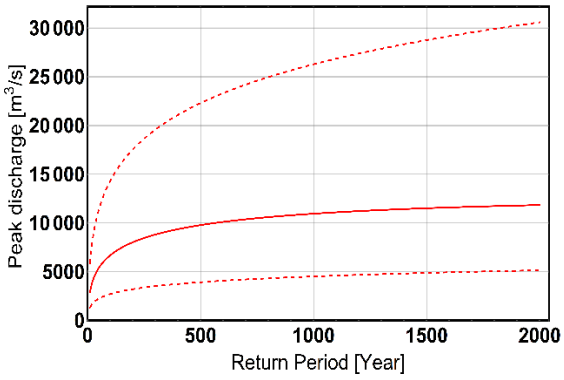

Table 2 Comparison of mean and 95% confidence interval of 150-year peak discharge distribution corresponding to the past experiment and 4K warmer experiment

Statistics in 150-year peak discharge	Past experiment	4 K warmer experiment	Change ratio 4 K warmer / Past
Mean	3960.0 [m^3/s]	7462.1 [m^3/s]	1.88
95% upper confidence limit value	7901.1 [m^3/s]	16171.3 [m^3/s]	2.04
95% lower confidence limit value	1858.0 [m^3/s]	2993.9 [m^3/s]	1.61

5 Summary

It is necessary to quantify the uncertainty of the design rainfall and establish a projection method for heavy rainfall in order to adapt to changing climate. In this joint research, the uncertainty of the design rainfall, which was derived from the observation of rainfall over the past several decades via traditional hydrological frequency analysis, was evaluated, and its future change was estimated by utilizing the huge amount of climate dataset. In particular, the ensemble climate data allowed us to quantify the uncertainty of the design rainfall and its confidence intervals due to the finite sample size of observations, as well as to evaluate the characteristics of the spatiotemporal rainfall pattern and the occurrence risk of large-scale heavy rainfall under climate change. In addition to the evaluation of the uncertainty in the total amount of rainfall, it is necessary to incorporate the spatiotemporal distribution of rainfall into flood control, because the shape of the hydrograph and peak discharge are affected by the distribution of rainfall pattern, even for the same volume of rainfall. Therefore, we have developed a framework for understanding the rainfall–peak discharge relation and evaluating its impact on the probable discharge.

In flood control management, flood control facilities such as levees and retarding basins are planned by considering the design peak discharge and water level, which are calculated through a hydrological model using the hyetograph of design rainfall. In working package 1, a framework to estimate the probability distribution of peak discharge with a target design return period that can incorporate the spatiotemporal distribution of rainfall is proposed. Specifically, the probability distribution of rainfall corresponding to the target return period is transformed into the probability distribution of peak discharge through the relationship between total rainfall and peak discharge, which is defined by rainfall characteristic and rainfall-runoff model. The distribution of the probable rainfall derived from the ensemble climate data and the total rainfall–peak discharge relation specified by the rainfall-runoff model were used as inputs to calculate the probable peak discharge. Therefore, the methodology can be used to update the probability distribution of peak discharge with the target design return period, in accordance with the differences and sophistication of climate models and rainfall-runoff models; this can contribute to the realization of flood risk assessment in response to future advances in science and technology.

6 Reference

1. Bas Kolen and Ira Helsloot, 2012: Time needed to evacuate the Netherlands in the event of large-scale flooding: strategies and consequences.
2. Beven, K.J., M.J. Kirkby, N. Schofield, A.F. Tagg, 1984: Testing a physically-based flood forecasting model (TOPMODEL) for three U.K. catchments, J. Hydrol, Volume 69, Issues 1–4, Pages 119-143, ISSN 0022-1694, https://doi.org/10.1016/0022-1694(84)90159-8.
3. David Samuel Williams, María Máñez Costa, Dmitry Kovalevsky, Bart van den Hurk, Bastian Klein, Dennis Meißner, Manuel Pulido-Velazquez, Joaquín Andreu, Sara Suárez-Almiñana, A method of assessing user capacities for effective climate services, Climate Services, Volume 19, 2020, 100180, ISSN 2405-8807, https://doi.org/10.1016/j.cliser.2020.100180.
4. Kain, J.S.; Fritsch, J.M. 1993: Convective Parameterization for Mesoscale Models: The Kain-Fritsch Scheme. In The Representation of Cumulus Convection in Numerical Models; Emanuel, K.A., Raymond, D.J., Eds.; Meteorological Monographs; American Meteorological Society: Boston, MA, USA; pp. 165–170.
5. Kawase, H.; Sasai, T.; Yamazaki, T.; Ito, R.; Dairaku, K.; Sugimoto, S.; Sasaki, H.; Murata, A.; Nosaka, M. , 2018: Characteristics of Synoptic Conditions for Heavy Snowfall inWestern to Northeastern Japan Analyzed by the 5-km Regional Climate Ensemble Experiments. J. Meteorol. Soc. Jpn., 96, 161–178.
6. Hoshino, T., Yamada, T. J., and Kawase, H., 2020: Evaluation for Characteristics of Tropical Cyclone Induced Heavy Rainfall over the Sub-basins in The Central Hokkaido, Northern Japan by 5-km Large Ensemble Experiments. Atmosphere, 11(435), 1–11.
7. Hirahara, S. Ishii, M. Fukuda, Y., 2014: Centennial-Scale Sea Surface Temperature Analysis and Its Uncertainty. J. Clim., 27, 57–75.
8. Hiroyasu YASUDA, Masami SHIRATO, Chiaki GOTO and Tadashi YAMADA, 2003: Development of Rapid Numerical Inundation Model for the Levee Protection Activity, Journal of Japan society civil engineering, No. 740/II-64, 1-17.
9. Intergovernmental Panel on Climate Change 2021. Sixth Assessment Report.
10. Jonkman, S.N., 2007: Loss of life estimation in flood risk assessment; theory and applications, TU, Delft, library.
11. Khaing, Z.M.; Zhang, K.; Sawano, H.; Shrestha, B.B.; Sayama, T.; Nakamura, K.,2019: Flood hazard mapping and assessment in data-scarce Nyaungdon area, Myanmar. PLoS ONE 2019, 14. DOI:10.1371/journal.pone.0224558.
12. KNMI, Deltares.,2015: Wat Betekenen de Nieuwe Klimaatscenario's voor de Rivierafvoeren van Rijn en Maas?. p. 15., Available online: http://publications.deltares.nl/1220042_004.pdf (accessed on 4 September 2020).

13. Koirala, S., Yeh, P.J.F., Hirabayashi, Y., Kanae, S., Oki, T., 2014: Global-scale land surface hydrologic modeling with the representation of water table dynamics. J. Geophys. Res. 119, 75–89. https://doi.org/10.1002/2013JD020398
14. Maaskant, B. et al., 2009: Analysis slachtofferaantallen VNK-2 en voorstellen voor aanpassingen van slachtooerfuncties,4-40.
15. Moriguti, S., 1995: Testing Hypothesis on Probability Representing Function—Kolmogorov–Smirnov Test Reconsidered. Jpn. J. Stat. Data Sci., 25, 233–244.
16. Mizuta, R.; Yoshimura, H.; Murakami, H.; Matsueda, M.; Endo, H.; Ose, T.; Kamiguchi, K.; Hosaka, M.; Sugi, M.; Yukimoto, S.; et al., 2012: Climate Simulations Using MRI-AGCM3.2 with 20-km Grid. J. Meteorol. Soc. Jpn., 90, 233–258.
17. Ministry of Land, Infrastructure, Transport, and Tourism (MLIT)., 2017. Flood Control Technology Review Meeting Considering the Climate Change in Hokkaido Region. Available online: https://www.hkd.mlit.go.jp/ky/kn/kawa_kei/splaat000001offi.html
18. Ministry of Land, Infrastructure, Transport, and Tourism (MLIT). Flood Control Technology Review Meeting Considering the Climate Change in Hokkaido Region. Available online: https://www.hkd.mlit.go.jp/ky/kn/kawa_kei/splaat000001offi.html
19. Nguyen-Le, D., Yamada, T. J., 2017: Simulation of tropical cyclone 201610 (Lionrock) and its remote effect on heavy rainfall in Hokkaido. Journal of Japan Society of Civil Engineers, Ser. B1 (Hydraulic Engineering), 73(4), I_199-I_204.
20. Nguyen T.T.; Nakatsugawa, M.; Yamada, T.J.; Hoshino, T.,2021: Flood inundation assessment in the low-lying river basin considering extreme rainfall impacts and topographic vulnerability. Water., 13, 896-. DOI:10.3390/w13070896.
21. Pokhrel, Y.N., Felfelani, F., Shin, S., Yamada, T.J., Satoh, Y., 2017: Modeling large-scale human alteration of land surface hydrology and climate. Geosci. Lett. 4. https://doi.org/10.1186/s40562-017-0076-5
22. Sasaki, H.; Kurihara, K.; Takayabu, I.; Uchiyama, T., 2008: Preliminary Experiments of Reproducing the Present Climate Using the Non-hydrostatic Regional Climate Model. Sola, 4, 25–28.
23. Taylor, K.E.; Stouer, R.J.; Meehl, G.A., 2012: An Overview of CMIP5 and the Experiment Design. Bull. Am. Meteorol. Soc., 93, 485–498.
24. Sayama, T.; Ozama, G.; Kawakami, T.; Nabesaka, S.; Fukami, K., 2012: Rainfall-runoffinundation analysis of the 2010 Pakistan flood in the Kabul River basin. Hydro. Sci. J., 57, 298–312. DOI:10.1080/02626667.2011.644245
25. Sayama, T.; Tatebe, Y.; Iwami, Y.; Tanaka, S., 2015: Hydrologic sensitivity of flood runoff and inundation: 2011 Thailand floods in the Chao Phraya River basin. Nat. Hazards Earth Syst. Sci. ,15, 1617–1630. DOI:10.5194/nhess-15-1617-2015.

26. Shimizu, K., Yamada, T. J., and Yamada, T., 2020: Uncertainty Evaluation in Hydrological Frequency Analysis Based on Confidence Interval and Prediction Interval. Water, 12(9):2554
27. Takata, K., Emori, S., Watanabe, T., 2003: Development of the minimal advanced treatments of surface interaction and runoff. Glob. Planet. Change 38, 209–222. https://doi.org/10.1016/S0921-8181(03)00030-4
28. The Ministry of infrastructure and Environment and The Ministry of Economic Affairs, 2015: National Water Plan 2016-2021.
29. Try, S.; Tanaka, S.; Tanaka, K.; Sayama, T.; Lee, G.; Oeurng, C., 2020: Assessing the effects of climate change on flood inundation in the lower Mekong Basin using high resolution AGCM outputs. Prog. Earth Planet. Sci, 7, 34. DOI:10.1186/s40645-020-00353-z.
30. Van alphen, J, 2016: The delta programme and updated flood risk management policies in the Netherlands, 9.
31. Yamada, T. J., Hoshino, T., and Suzuki, A. 2021: Using a massive high‐resolution ensemble climate data set to examine dynamic and thermodynamic aspects of heavy precipitation change. Atmospheric Science Letters, (July), 1–11.
32. Yamada, T. J., 2019：Adaptation Measures for Extreme Floods Using Huge Ensemble of High－Resolution Climate Model Simulation in Japan. Summary Report on the Eleventh Meeting of the Research Dialogue 2019，28－30，UNFCCC Bonn Climate Change Conference, Bonn, Germany（June 19 2019）
33. Yamada, T. J., 2020：Ensemble Approach to Climate Change Projection and Risk Assessment, KASEN (RIVER), pp.77-81,Japan River Association.
34. Yamada, T.J.; Hoshino, T.; Masuya, S.; Uemura, F.; Yoshida, T.; Omura, N.; Yamamoto, T.; Chiba, M.; Tomura, S.; Tokioka, S.; et al.,2018: The influence of climate change on flood risk in Hokkaido. Adv. River Eng., 24, 391–396.
35. Yamazaki, D., Kanae, S., Kim, H., Oki, T., 2011. A physically based description of floodplain inundation dynamics in a global river routing model. Water Resour. Res. 47, 1–21. https://doi.org/10.1029/2010WR009726

Head office
HKV
Botter 11-29
8232 JN Lelystad
The Netherlands

Branch office
Informaticalaan 8
2628 ZD Delft
The Netherlands

+31 320 294242
info@hkv.nl
www.hkv.nl/en/